

**Collisions of three-dimensional bipolar optical solitons in an array of carbon nanotubes**

Alexander V. Zhukov and Roland Bouffanais\*

*Singapore University of Technology and Design, 8 Somapah Road, 487372 Singapore*

Boris A. Malomed

*Department of Physical Electronics, School of Electrical Engineering,  
Faculty of Engineering, Tel Aviv University, 69978 Tel Aviv, Israel*

Hervé Leblond

*LUNAM Université, Université d'Angers, Laboratoire de Photonique d'Angers,  
EA 4464, 2 Boulevard Lavoisier, 49000 Angers, France*

Dumitru Mihalache

*Academy of Romanian Scientists, 54 Splaiul Independentei, Bucharest, RO-050094, Romania and  
Horia Hulubei National Institute of Physics and Nuclear Engineering, Magurele, RO-077125, Romania*

Eduard G. Fedorov

*Department of Biology, Technion-Israel Institute of Technology, Haifa 32000, Israel and  
Vavilov State Optical Institute, 199053 Saint Petersburg, Russia*

Nikolay N. Rosanov

*Vavilov State Optical Institute, 199053 Saint Petersburg, Russia  
Saint Petersburg National Research University of Information Technologies,  
Mechanics and Optics (ITMO University), 197101 Saint Petersburg, Russia and  
Ioffe Physical-Technical Institute, Russian Academy of Sciences, 194021 Saint Petersburg, Russia*

Mikhail B. Belonenko

*Laboratory of Nanotechnology, Volgograd Institute of Business, 400048 Volgograd, Russia and  
Volgograd State University, 400062 Volgograd, Russia*

(Dated: November 16, 2016)

We study interactions of extremely short three-dimensional bipolar electromagnetic pulses propagating towards each other in an array of semiconductor carbon nanotubes, along any direction perpendicular to their axes. The analysis provides a full account of the effects of the nonuniformity of the pulses' fields along the axes. The evolution of the electromagnetic field and charge density in the sample is derived from the Maxwell's equations and the continuity equation, respectively. In particular, we focus on indirect interaction of the pulses via the action of their fields on the electronic subsystem of the nanotube array. Changes in the shape of pulses in the course of their propagation and interaction are analyzed by calculating and visualizing the distribution of the electric field in the system. The numerical analysis reveals a possibility of stable post-collision propagation of pulses over distances much greater than their sizes.

PACS numbers: 42.65.Tg, 42.65.Sf, 78.67.-n, 78.67.Ch

**I. INTRODUCTION**

Among materials which have been drawing a permanently strong interest in the course of the last three decades are carbon nanotubes (CNTs). They are considered as one of the most promising semiconductor materials for developing a new element base of electronics. CNTs are macromolecular objects, in the form of layers of graphene rolled into a cylinder, the surface of which is formed by six carbon cycles [1]. Nanotubes can be single

walled or multi-walled, if the tube is composed of one or several layers of graphene, respectively. The CNTs are categorized as chiral, if angles between sides of the hexagons and nanotube axis are different from  $0^\circ$  and  $90^\circ$ , and achiral otherwise. Further, achiral CNTs exhibit two different structures: "saddles," if the sides of the hexagons are perpendicular to the nanotube axis, or "zigzags," with a parallel arrangement of the hexagons relative to the axis.

Since the discovery of nanotubes by Iijima [2, 3] and up to now, a great deal of work has been done on the synthesis and characterization of different types of CNTs (see reviews [4–8] and references therein). There are de-

---

\* Corresponding Author: bouffanais@sutd.edu.sg

tailed descriptions of physical properties of CNTs, as defined by their geometry and surface structure, i.e., the arrangement of the hexagonal carbon cycles relative to the axis of the nanotube. Calculations of the band structure show that, depending on their build, the CNT may feature metallic, insulating, or semiconductor properties, that offer a great potential for applications [1, 4]. Peculiarities of the electron energy spectrum of semiconductor single-walled CNTs of the zigzag type (see Refs. [8, 9]) are manifestations of a number of nonlinear electrodynamic properties similar to those in semiconductors with a superstructure, for instance, in quantum semiconductor superlattices [11, 12]. Non-quadratic electron dispersion suggests a possibility of realization (in electric fields of moderate strength  $\sim 10^3$ – $10^5$  V/cm) of diverse nonlinear phenomena, such as nonlinear and absolute negative conductivity [13, 14], phase transitions of the first kind induced by the applied external field [14], nonlinear diffraction and self-focusing of laser beams [15, 16], electromagnetic solitary waves [17], etc.

A wide range of applications to modern optoelectronics may stem from these phenomena. Moreover, the recent advancement of laser physics in the generation of powerful electromagnetic radiation, including pulses of ultrashort duration with predetermined parameters [18–23], is an incentive for a comprehensive study of the propagation of nonlinear electromagnetic waves, including extremely short pulses, in settings based on CNTs. It was first predicted theoretically in Ref. [17] that the propagation of electromagnetic solitary waves in CNT arrays is possible in a one-dimensional (1D) model. Later, these results have been extended to more realistic multidimensional models. In particular, detailed studies of the propagation of two-dimensional (2D) unipolar and bipolar extremely short electromagnetic pulses in CNT arrays have been carried out (see Refs. [24–26]). Three-dimensional (3D) spatiotemporal optical solitons (“light bullets” [27–29]) have been considered too [30].

Actual samples may contain various chemical impurities and structural defects, both intentionally produced ones or resulting from manufacture imperfections. The chemical impurities are uniformly distributed over a CNT array, affecting the dynamics of extremely short electromagnetic pulses [31–33]. In Refs. [34–36], a detailed analysis has been developed for the propagation of unipolar solitary waves in a medium with metallic inclusions, while Ref. [37] established the selective nature of the interaction of an extremely short bipolar electromagnetic pulse with a spot featuring higher concentration of electrons, induced by a local dopant. Moving towards a more realistic description of the solitary electromagnetic waves in CNT arrays, one should gradually increase the complexity of the underlying model by considering factors that may occur in experimental situations. Along with the possible presence of static heterogeneities in the medium, such as, for example, the local inhomogeneity of the conduction-electron density, it was found necessary to address the shape of the field of propagating electromag-

netic pulses in 2D and 3D models (see Ref. [38] and references therein). The distribution of the electric field along the CNT axis causes, in turn, redistribution of the concentration of conduction electrons in the medium. Thus, in general, there is another possible type of heterogeneity of the medium, namely, the dynamic inhomogeneity induced by the field of the propagating electromagnetic waves. Effects associated with this type of the induced heterogeneity have never been thoroughly investigated, to the best of our knowledge.

Obviously, each electromagnetic pulse propagating in the medium is affected by the spatiotemporal perturbation, induced by the “trace” of the inhomogeneous distribution of the electron density caused by the passage of other pulses in the vicinity of a given one (see Sec. IID). Therefore, it is relevant to consider the propagation of extremely short electromagnetic pulses in the presence of a dynamical inhomogeneity induced by the fields of other pulses. This problem also has relevance to possible applications based on multiple rapid passages of electromagnetic pulses through the specimen.

In this vein, this work deals with collisions of 3D extremely short bipolar pulses (light bullets), taking into account the interaction of each one with perturbations of the electron density induced by the field profile of the other pulse. The analysis aims to address the collisions in the form close to that observed in real experiments.

## II. GENERAL CONSIDERATIONS

### A. Geometry of the problem and restrictions of the model

To begin with, we have to clarify the term “soliton” used in this paper. Strictly speaking, we do not provide a mathematical proof for the ultrashort waves we consider as being solitons (see Appendix A for the outline of this problem). Specifically, we consider the propagation of a solitary electromagnetic wave (infrared laser pulse) through a volumetric array of semiconductor CNTs forming a monolayer of the zigzag type,  $(m, 0)$ , where integer  $m$  (different from a multiple of three) is the number of hexagonal carbon cycles which form the circumference of the nanotube. The second integer is the pitch of the helical pattern, also measured as the respective number of hexagonal carbon cycles, it is zero for a zigzag CNT. Integer  $m$  further determines the CNT radius, as  $R = m\sqrt{3}b/(2\pi)$ , where  $b = 1.42 \times 10^{-8}$  cm is the distance between nearest-neighbor carbon atoms [8, 9]. The CNTs are supposed to be placed into a homogeneous insulator, so that axes of the nanotubes are parallel to the common  $x$  axis, and distances between adjacent nanotubes are much larger than their diameter, allows one to neglect the interaction between CNTs [39] (see Fig. 1). In particular, with this configuration one can neglect the electron inter-hopping, supposing that the corresponding wave functions do not overlap, which is important in

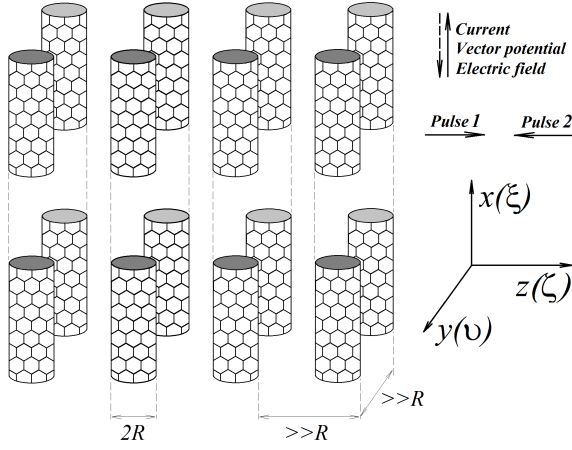


FIG. 1. The schematic diagram of the setup with associated coordinate system.

order to avoid uncontrollable transverse currents. The CNT radius is  $R \simeq 5.5 \times 10^{-8}$  cm for  $m = 7$ , which is the value adopted in the computations below. It is very small in comparison with the radiation wavelength in the infrared range, which exceeds  $10^{-4}$  cm.

Essentially, the chosen geometry of the problem is similar to the one considered in Refs. [30, 38]. Given this framework, the dispersion relation for energy  $\epsilon$  of conduction electrons of CNTs is [8, 9]

$$\epsilon(p_x, s) = \gamma_0 \sqrt{1 + 4 \cos\left(p_x \frac{d_x}{\hbar}\right) \cos\left(\pi \frac{s}{m}\right) + 4 \cos^2\left(\pi \frac{s}{m}\right)}, \quad (1)$$

where the electron quasimomentum is  $\mathbf{p} = \{p_x, s\}$ ,  $s$  being an integer characterizing the momentum quantization along the perimeter of the nanotube,  $s = 1, 2, \dots, m$ ,  $\gamma_0$  is the overlap integral, and  $d_x = 3b/2$  [10]. In this paper, we consider the propagation of extremely short 3D pulses in direction  $z$  perpendicular to CNT axis  $x$ , with the electric field of the pulses oriented along the  $x$  axis (see details below). The duration of each pulse is assumed to be much smaller than the electron relaxation time  $t_{\text{rel}}$ , which makes it possible to limit the evolution

time to  $t < t_{\text{rel}}$  [see Eq. (24) below], allowing one to consider the evolution of the electromagnetic field in the collisionless approximation [30].

## B. Equation for the vector potential

We treat the electromagnetic field in the CNT array by means of the Maxwell's equations [40, 41] in terms of the vector and scalar potentials,  $\mathbf{A}$  and  $\phi$ . In the chosen geometry, the governing equation for the vector potential in the Lorentz gauge is

$$\frac{\epsilon}{c^2} \frac{\partial^2 \mathbf{A}}{\partial t^2} - \frac{\partial^2 \mathbf{A}}{\partial x^2} - \frac{\partial^2 \mathbf{A}}{\partial y^2} - \frac{\partial^2 \mathbf{A}}{\partial z^2} = \frac{4\pi}{c} \mathbf{j}, \quad (2)$$

with  $\mathbf{A} = \{A(x, y, z, t), 0, 0\}$ ,  $\mathbf{j} = \{j(x, y, z, t), 0, 0\}$  is the current density,  $\epsilon$  is the average relative dielectric constant of the medium [11], and  $c$  is the speed of light in vacuum. The choice of the vector potential in the CNT collinear to the axes of the nanotubes is justified by the following considerations. According to the formulation of the problem, the array has a nonzero electrical conductivity only along the  $x$  axis, while the conduction current is negligible in the  $(y, z)$  plane, given the vanishingly small interactions between the nanotubes, hence, the current density is defined as  $\mathbf{j} = \{j(x, y, z, t), 0, 0\}$ . In this case, Eq. (2) allows to nullify the second and third components of the vector potential,  $\mathbf{A} = \{A(x, y, z, t), 0, 0\}$ .

Expanding the electron energy spectrum (1) into a Fourier series, and bearing in mind that the electrons obey the Fermi-Dirac statistics, we apply the technique developed in Refs. [44, 45], which makes it possible to produce an expression for the projection of the current density onto the CNT axis in the following form (see Appendix B for details):

$$j = -en \frac{d_x}{\hbar} \gamma_0 \sum_{r=1}^{\infty} G_r \sin \left[ r \frac{d_x}{\hbar} \left( A \frac{e}{c} + e \int_0^t \frac{\partial \phi}{\partial x} dt' \right) \right], \quad (3)$$

where  $e$  is the electron charge ( $e < 0$ ),  $n$  the concentration of conduction electrons in the array,  $\phi$  the scalar potential, and coefficients  $G_r$  are given by

$$G_r = -r \frac{\sum_{s=1}^m \frac{\delta_{r,s}}{\gamma_0} \int_{-\pi}^{+\pi} \cos(r\kappa) \left\{ 1 + \exp \left[ \frac{\theta_{0,s}}{2} + \sum_{q=1}^{\infty} \theta_{q,s} \cos(q\kappa) \right] \right\}^{-1} d\kappa}{\sum_{s=1}^m \int_{-\pi}^{+\pi} \left\{ 1 + \exp \left[ \frac{\theta_{0,s}}{2} + \sum_{q=1}^{\infty} \theta_{q,s} \cos(q\kappa) \right] \right\}^{-1} d\kappa}. \quad (4)$$

Here,  $\theta_{r,s} = \delta_{r,s} (k_B T)^{-1}$ ,  $T$  is the temperature,  $k_B$  the Boltzmann constant, and  $\delta_{r,s}$  are coefficients of the

Fourier decomposition of spectrum (1):

$$\delta_{r,s} = \frac{d_x}{\pi \hbar} \int_{-\pi \hbar / d_x}^{-\pi \hbar / d_x} \epsilon(p_x, s) \cos \left( r \frac{d_x}{\hbar} p_x \right) dp_x. \quad (5)$$

Next, we combine Eqs. (2) and (3) to derive an equation

governing the evolution of the vector potential in the CNT array, in the dimensionless notation:

$$\frac{\partial^2 \Psi}{\partial \tau^2} - \left( \frac{\partial^2 \Psi}{\partial \xi^2} + \frac{\partial^2 \Psi}{\partial v^2} + \frac{\partial^2 \Psi}{\partial \zeta^2} \right) + \eta \sum_{r=1}^{\infty} G_r \sin \left[ r \left( \Psi + \int_0^{\tau} \frac{\partial \Phi}{\partial \xi} d\tau' \right) \right] = 0, \quad (6)$$

where  $\eta = n/n_0$  is the scaled electron concentration,  $n_0$  being the equilibrium concentration in a homogeneous specimen in the absence of the electromagnetic field,  $\Psi = Aed_x/(c\hbar)$  is the projection of the scaled vector potential onto the  $x$  axis,  $\Phi = \phi\sqrt{\varepsilon}ed_x/(c\hbar)$  is the dimensionless scalar potential,  $\tau = \omega_0 t/\sqrt{\varepsilon}$  is the scaled time,  $\xi = x\omega_0/c$ ,  $v = y\omega_0/c$  and  $\zeta = z\omega_0/c$  are the scaled coordinates, and

$$\omega_0 \equiv 2 \frac{|e|d_x}{\hbar} \sqrt{\pi\gamma_0 n_0}. \quad (7)$$

Equation (7) determines a characteristic angular frequency of the CNT electron subsystem in the conduction band, which is similar to the plasma frequency of electrons in semiconductor superlattices, cf. Ref. [11].

### C. The equation for the scalar potential field

Fields of extremely short electromagnetic pulses under consideration are localized in all the three directions of the Cartesian coordinates system. The nonuniformity of the field along the direction perpendicular to the CNT axis has no impact on the distribution of the electron concentration in the sample, as the interaction between the nanotubes is negligible, and, as said above, there is no electric current in the  $(y, z)$  plane. On the contrary, the field nonuniformity along the  $x$  axis perturbs the conduction-current density, which, in turn, affects the charge density in the sample [30, 38]. In this connection, we note that concentration  $n$  of the conduction electrons in the expression for the conduction current (3) and, consequently, the scaled electron concentration,  $\eta$ , are, in general, functions of the coordinates and time,  $\eta = \eta(\xi, v, \zeta, \tau)$ .

Obviously, the redistribution of the electron density leads to a change of the scalar potential. The Maxwell's equations [40, 41] produce an evolution equation for the scalar potential (see also Ref. [30]):

$$\frac{\partial^2 \Phi}{\partial \tau^2} - \left( \frac{\partial^2 \Phi}{\partial \xi^2} + \frac{\partial^2 \Phi}{\partial v^2} + \frac{\partial^2 \Phi}{\partial \zeta^2} \right) = \beta(\eta - 1), \quad (8)$$

where  $\beta = c\hbar/(d_x\gamma_0\sqrt{\varepsilon})$ .

### D. Equation for the electron density

As mentioned above, the nonuniformity of the electric field along the CNT axis ( $x$ ) perturbs the current density in this direction, as follows from Eq. (3), leading to redistribution of the electron density. The total charge in the sample being conserved, the change in the bulk charge density,  $\rho = en$ , obeys the continuity equation,  $\nabla \cdot \mathbf{j} + \partial\rho/\partial t = 0$  [40, 41]. Projected onto the CNT axis, this equation reads as

$$\frac{\partial j}{\partial x} + \frac{\partial \rho}{\partial t} = 0. \quad (9)$$

Substituting Eq. (3) into Eq. (9), and passing to the dimensionless notation, we obtain an evolution equation for the electron concentration under the action of the pulse's electromagnetic field:

$$\frac{\partial \eta}{\partial \tau} = \alpha \sum_{r=1}^{\infty} G_r \frac{\partial}{\partial \xi} \left\{ \eta \sin \left[ r \left( \Psi + \int_0^{\tau} \frac{\partial \Phi}{\partial \xi} d\tau' \right) \right] \right\}, \quad (10)$$

where  $\alpha \equiv d_x\gamma_0\sqrt{\varepsilon}/c\hbar$ . It is worth noting that the nonlinearity of the concentration of electrons [see Eq. (10)] bears the same nature as the nonlinearity of the current density [see Eq. (3)], the latter being responsible for the reshaping of the electron concentration. Furthermore, the accumulation of charge is a direct consequence of the inhomogeneity of the current along the CNTs. Accordingly, an additional electric field can appear, which is fully accounted for in this study.

Thus, the evolution of the field in the array, taking into regard the perturbation of the conduction-electron density due to the nonuniformity of the field along the CNT axis, is governed by Eqs. (6), (8), and (10). This is a self-consistent system for the coupled evolution of the field and electron density: the field impacts the dynamics of electrons, and the latter's feedback affects the evolution of the field, which resembles the Vlasov's equations in plasma physics [42], and the recently studied local-field effect for the propagation of optical and microwave fields in atomic Bose-Einstein condensates [43].

### E. Characteristics of the pulse field

Measuring instruments can record the energy characteristics of the pulse defined by the electric field [46]. The

electric field in the CNT array is determined by the potentials,  $\mathbf{E} = -c^{-1}\partial\mathbf{A}/\partial\mathbf{t} - \nabla\phi$  [40, 41], which can be written using the dimensionless variables defined above:

$$\mathbf{E} = E_0 \left( \frac{\partial\Psi}{\partial\tau} + \frac{\partial\Phi}{\partial\xi}, \frac{\partial\Phi}{\partial v}, \frac{\partial\Phi}{\partial\zeta} \right), \quad (11)$$

$$E_0 \equiv -\frac{\hbar\omega_0}{ed_x\sqrt{\varepsilon}}. \quad (12)$$

Thus, Eq. (11) demonstrates that the electric field can be represented as a superposition of two components,  $\mathbf{E} = \mathbf{E}_{\parallel} + \mathbf{E}_{\perp}$ , where  $\mathbf{E}_{\parallel}$  is directed along the CNT axis,

$$\mathbf{E}_{\parallel} = E_0 \left( \frac{\partial\Psi}{\partial\tau} + \frac{\partial\Phi}{\partial\xi}, 0, 0 \right), \quad (13)$$

and  $\mathbf{E}_{\perp}$  is the electric field in the orthogonal plane,

$$\mathbf{E}_{\perp} = E_0 \left( 0, \frac{\partial\Phi}{\partial v}, \frac{\partial\Phi}{\partial\zeta} \right). \quad (14)$$

Electric field  $\mathbf{E}_{\perp}$  has no effect on the dynamics of electrons due to the absence of the conductivity in the  $(y, z)$  plane. Expression (14) shows that field  $\mathbf{E}_{\perp}$  appears due to the perturbation of the conduction-electrons density and the presence of the scalar potential. This field is determined by the projection of vector  $-\nabla\phi$  onto the  $(y, z)$  plane. In other words, the nonuniformity of field  $\mathbf{E}_{\parallel}$  along the CNT axis gives rise to electric field  $\mathbf{E}_{\perp}$  in the orthogonal plane.

As the conductivity of the array is different from zero only along the  $x$  axis, the dynamics of the electron subsystem affects only electric field  $\mathbf{E}_{\parallel}$ , which, in turn, is itself generated by the dynamics of electrons. The interaction of field  $\mathbf{E}_{\parallel}$  with the electron subsystem gives rise to a self-consistent field of the electromagnetic solitary wave. To visualize the distribution of the wave field and identify its localization, we introduce  $I = I(\xi, v, \zeta, \tau) \equiv |\mathbf{E}_{\parallel}|^2 / (8\pi)$ . It has the dimension of the volume energy density [40, 41], therefore we call it the bulk energy density of the electric field of the wave. Following Eqs. (12) and (13), it may be expressed as

$$I = I_0 \left( \frac{\partial\Psi}{\partial\tau} + \frac{\partial\Phi}{\partial\xi} \right)^2, \quad (15)$$

where  $I_0 = (\hbar\omega_0)^2 / (e^2 d_x^2 8\pi\varepsilon)$ . Numerical calculations reveal that the profile of  $I(\xi, v, \zeta, \tau)$  may feature pronounced maxima, whose positions at any given moment in time are identified as position of the solitary waves.

## F. Methodological aspects

Concluding this section, we would like to specify two aspects which, from a methodological point of view, may be useful for modeling wave phenomena in nonlinear media. In general, there are at least two different approaches

to the analysis of the problem. The primary focus here is on the mathematical scheme based upon the Fourier expansion of dispersion relation (1) (see Appendix B), and we here explain the feasibility of this approach. Current density (3) determines Eq. (6) for the vector potential field, and Eq. (10) for the electron concentration. We stress that the expression for current density (3), and therefore Eqs. (6) and (10), does not contain any explicit dependencies following from the particular form of function  $\epsilon(p_x, s)$ . In other words, for any medium, defined by its electron dispersion, which may be different from Eq. (1), the current density will be expressed similarly to Eq. (3). At the same time, properties of the specific environment, determined by its electron energy spectrum, will affect the expression for the current density through coefficients similar to  $G_{r,s}$ . Thus, deriving equations describing the evolution of electromagnetic waves in an the CNT array, we also derive a universal approach for optimizing simulations of the wave propagation in generic media defined by the energy dependence of the conduction electrons on their quasimomenta. Given that the equations for the current density and vector potential have been derived, one can select a numerical scheme for solving the corresponding system of equations, this scheme remaining effective for other environments. Of course, a particular medium comes with a specific electron-energy spectrum, thus leading to different values of coefficients similar to those in Eq. (4), which determine the Fourier decomposition of the spectrum. Nonetheless, the actual form of the governing equation [similar to Eqs. (6) and (10)], and the type of the numerical scheme remain the same.

There is another approach to the visualization of the pulse evolution, which can be combined with the one proposed above. Intensity  $I(\xi, v, \zeta, \tau)$  given by Eq. (15) yields the distribution of the electric-field energy of the pulse at a fixed instant of time. However, neither the distribution of the electric field, nor the distribution of the field's energy density at a given moment of time determine the direction of motion of electromagnetic pulses. In other words, when plotting the distribution  $I(\xi, v, \zeta, \tau)$  at a particular moment of time, one cannot directly know in what direction the electromagnetic waves propagate, without having at least one similar plot at another moment of time. However, there is a method for identifying the propagation direction of the electromagnetic pulse at time  $\tau$  without calculating the distribution of  $I(\xi, v, \zeta, \tau)$  at time  $\tau + d\tau$ . Namely, one can supplement  $I(\xi, v, \zeta, \tau)$  at time  $\tau$  by Poynting vector  $\mathbf{S} = \{S_x, S_y, S_z\}$  [40, 41] (see Appendix C).

The absolute value of the Poynting vector determines the magnitude of power flux carried by the field at each point of the CNT array at any instant of time. The direction of the power transfer is determined by the sign and magnitude of components of  $\mathbf{S}$ ;  $\text{sign}(S_x)$ ,  $\text{sign}(S_y)$ ,  $\text{sign}(S_z)$  and  $|S_x|$ ,  $|S_y|$ ,  $|S_z|$ , respectively. To explain this possibility, we resort to the simple example of the wave propagating along the  $z$  axis. The propagation of

the electromagnetic pulse in the positive direction of  $z$  is associated with the transfer of energy in this direction, which implies a positive Poynting-vector component  $S_z$ . Accordingly, the propagation in the negative direction is associated with  $S_z < 0$ . Thus, quantities  $I(\xi, v, \zeta, \tau)$  and  $S_z(\xi, v, \zeta, \tau)$  complement each other in drawing the complete structure of the electromagnetic field at any given moment:  $I(\xi, v, \zeta, \tau)$  determines the spatial localization of the electromagnetic field (i.e., the state of the system at time  $\tau$ ), while a particular component of the Poynting vector identifies the direction and intensity of the field-energy transfer along the respective axis, making it possible to predict the state of the system at time  $\tau + d\tau$ .

### III. NUMERICAL RESULTS

#### A. System's parameters and initial conditions

We assume that initially (at time  $\tau = \tau_0$ ) the electron density is uniform with value  $n_0$ , while the scalar potential is zero throughout the sample. These initial conditions are similar to those used in Ref. [30]:

$$\eta(\xi, v, \zeta, \tau_0) = 1, \quad (16)$$

$$\Phi(\xi, v, \zeta, \tau_0) = 0. \quad (17)$$

Assuming that there are two electromagnetic pulses propagating towards each other in the CNT array, we define the initial projection of the vector-potential field of the pair of pulses as follows:

$$\Psi(\xi, v, \zeta, \tau_0) = \sum_{i=1}^2 \left\{ \Psi_i(\zeta, \tau_0) \exp \left[ -\frac{(\xi - \xi_{0i})^2 + (v - v_{0i})^2}{\lambda_i^2} \right] \right\}, \quad (18)$$

where  $\Psi_i(\zeta, \tau_0)$  is the corresponding profile of the projection of the  $i$ -th pulse onto the  $\xi$  axis at  $\xi = \xi_{0i}$  and

$v = v_{0i}$ , and  $\lambda_i$  is the dimensionless initial transverse half-width of the  $i$ -th pulse, while  $\xi_{0i}$  and  $v_{0i}$  are the coordinates of the pulses' centers at  $\tau = \tau_0$ . We have chosen the Gaussian profile of the input, given by Eq. (18), in the  $(\xi, v)$  plane due to its occurrence in various applications [15, 46, 47].

To further justify the choice of the initial profile of each electromagnetic pulse in the longitudinal ( $\zeta$ ) direction, we provide the following arguments relating to Eq. (6). First, as shown by numerical calculations, coefficients  $G_r$  [see Eq. (4)] rapidly decay with the increase of  $r$ . Therefore, we keep only the terms with  $r = 1$  in Eq. (6). Second, for the time being we only consider the variation of the field in the longitudinal direction, restricting ourselves to the 1D description with coordinate  $\zeta$  and accepting the assumption of uniformity of the field along the  $\xi$  and  $v$  axes. Third, the assumption of the uniformity of the field along the  $\xi$  axis allows us to neglect possible perturbation of the electron density (i.e., we have  $\eta \approx 1$ ). It follows from here that a single scalar potential keeps a constant value throughout the sample, i.e.,  $\partial\Phi/\partial\xi = 0$ . This conclusion also follows from Eq. (8), which for  $\eta = 1$  admits the trivial stationary solution,  $\Phi = 0$ . As a result, we reduce Eq. (6) to an evolution equation for the nonvanishing component of the vector potential:

$$\frac{\partial^2 \Psi}{\partial \tau^2} - \frac{\partial^2 \Psi}{\partial \zeta^2} + \sigma^2 \sin \Psi = 0, \quad (19)$$

where we define  $\sigma \equiv \sqrt{G_1}$ . Our calculations always produce  $G_1 > 0$ , hence,  $\sigma$  is real, with  $\sigma^2 > 0$ . Equation (19) has the form of the celebrated sine-Gordon equation, which gives rise to solutions in the form of a breather, i.e., an oscillating nontopological soliton [48]:

$$\Psi_B(\zeta, \tau) = 4 \arctan \left\{ \sqrt{\frac{1}{\Omega^2} - 1} \frac{\sin \left( \sigma \Omega \frac{\tau - (\zeta - \zeta_0)u/v}{\sqrt{1 - (u/v)^2}} \right)}{\cosh \left( \sigma [\tau u/v - (\zeta - \zeta_0)] \sqrt{\frac{1 - \Omega^2}{1 - (u/v)^2}} \right)} \right\}, \quad (20)$$

with  $\Omega \equiv \omega_B/\omega_0 < 1$ ,  $u$  being the speed of the pulse propagation,  $v = c/\sqrt{\varepsilon}$  the linear speed of the electromagnetic waves in the medium, while  $\zeta_0$  is the coordinate of the breather's center at  $\tau = \tau_0$ .

Note that Eq. (6) shares similarities with Eq. (19), and, in some sense, it may be treated as a non-1D inhomogeneous modified sine-Gordon equation. Since Eq. (19) generates breather solutions given by Eq. (20), one may expect a possibility for the propagation of similar solitary

waves generated by Eq. (6).

We assume that the CNT array is irradiated by two bipolar ultra-short electromagnetic pulses propagating towards each other, so that the vector-potential field of the pair of pulses is determined by Eq. (18), in which  $\Psi_i(\zeta, \tau_0)$  have a form similar to that in Eq. (20):

$$\Psi_i(\zeta, \tau_0) = 4 \arctan \left\{ \sqrt{\frac{1}{\Omega^2} - 1} \frac{\sin \chi_i}{\cosh \mu_i} \right\}, \quad (21)$$

$$\chi_i \equiv \sigma \Omega_i \frac{\tau_0 - (\zeta - \zeta_{0i})u_i/v}{\sqrt{1 - (u_i/v)^2}}, \quad (22)$$

$$\mu_i \equiv \sigma \left[ \frac{\tau_0 u_i}{v} - (\zeta - \zeta_{0i}) \right] \sqrt{\frac{1 - \Omega_i^2}{1 - (u_i/v)^2}}. \quad (23)$$

Here we use the term “bipolar” in the sense that the electromagnetic field changes its sign in the course of the pulse propagation. We emphasize that we choose the far separated initial (at  $\tau = \tau_0$ ) electromagnetic pulses, given by initial conditions (21), hence the interaction between them is initially negligible.

It is worth stressing that the use of 1D equation (19) relates solely to the choice of the longitudinal profile of the initial condition [specifically, in the form of Eq. (20)] while we stay in the general framework of the 3D model. Clearly, the system of governing equations (6), (8), and (10), with initial conditions (16), (17), (18), and (21), does not have exact analytical solutions. We have therefore conducted a numerical investigation of the interaction of the electromagnetic pulses in the CNT array. To simulate the system of governing equations, we employed an explicit finite-difference scheme previously used and detailed in Refs. [38, 49], which was generalized for this 3D setting. Difference scheme steps in both time and space were iteratively decreased twice until the solution became unchanged in the eighth decimal place, thereby ensuring both spatial and temporal convergence of the obtained solution. Thus, we have numerically found values of  $\Psi(\xi, v, \zeta, \tau)$ ,  $\Phi(\xi, v, \zeta, \tau)$ ,  $\eta(\xi, v, \zeta, \tau)$ , the energy density of the electric field, defined as per Eq. (15), and also the Poynting vector.

In our simulations, we used the following realistic values of the parameters:  $m = 7$ ,  $b = 1.42 \times 10^{-8}$  cm,  $\gamma_0 = 2.7$  eV,  $d_x \approx 2.13 \times 10^{-8}$  cm. The system is immersed into a medium with the relative dielectric constant  $\varepsilon = 4$ . We consider the system at room temperatures  $T = 293$  K, with the equilibrium electron concentration  $n_0 = 10^{18}$  cm $^{-3}$  [39]. As follows from Eq. (7),  $\omega_0 \approx 7.14 \times 10^{13}$  rad s $^{-1}$ ,  $\alpha$  and  $\beta$  in Eqs. (8) and (10) take values  $\alpha \approx 5.8 \times 10^{-3}$  and  $\beta \approx 1.72 \times 10^2$ , while  $\sigma = 0.95$  in Eqs. (22) and (23). Note also that our results are obtained in the framework of the collisionless model, which is valid at times not exceeding the above-mentioned relaxation time:

$$t < t_{\text{rel}} \approx 3 \times 10^{-13} \text{ s} \quad (24)$$

[9], which may be sufficient to complete the collision between the pulses.

The parameters of the electromagnetic pulses,  $u_i/v$ ,  $\Omega_i$ , and  $\lambda_i$ , were varied in a wide range, similar to what was done previously in Ref. [30]. To be specific, we here present typical results for the following initial parameters:  $u_1/v = -u_2/v = 0.95$ ,  $\Omega_{1,2} = 0.5$ , which corresponds to a half-cycle pulse with vacuum wavelength  $\approx 16 \mu\text{m}$ , belonging to the long-wavelength infrared range, and  $\lambda_{1,2} = 2$ ,  $\xi_{01,2} = v_{01,2} = 0$ ,  $\zeta_{02} = -\zeta_{01} = 3$ . Note that, because of our choice of the initial conditions, the

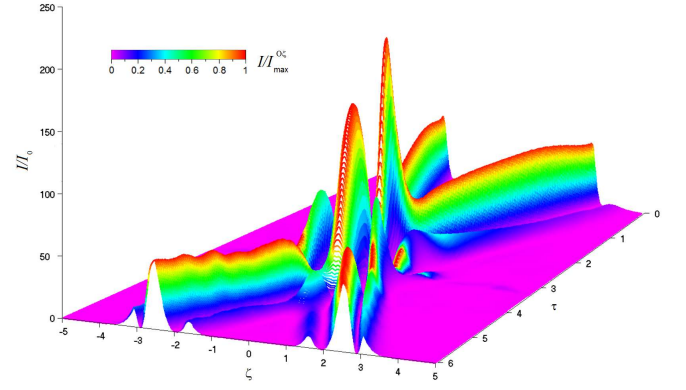


FIG. 2. The evolution of the energy density  $I(\xi = 0, v = 0, \zeta, \tau)$  of the electric field on the  $\zeta$  axis. Values of  $I$  at every instant of time are color coded, with red and purple corresponding to maxima and minima.

centers of the electromagnetic pulses,  $(\xi_{01}, v_{01}, \zeta_{01})$  and  $(\xi_{02}, v_{02}, \zeta_{02})$ , are initially located on the  $\zeta$  axis.

## B. Interactions of the electromagnetic pulses

Figures 2–5 display results of the 3D simulations of the interaction of bipolar laser pulses in the CNT array with the parameters defined in the previous subsection. Figure 2 shows the evolution of the energy density distribution of the electric field,  $I(0, 0, \zeta, \tau)$ , in the array in the course of the propagation and interaction of the pulses along the  $\zeta$  axis, i.e., in the case of  $\xi_{01,2} = v_{01,2} = 0$ . With the value of  $\omega_0$  chosen above, the length unit on the  $\zeta$  axis corresponds to a distance  $c/\omega_0 \approx 4 \times 10^{-4}$  cm in physical units, hence, the coordinate interval shown in the figure,  $|\zeta| \leq 5$ , corresponds to distance  $\Delta z \approx 4 \times 10^{-3}$  cm. Further, the unit of dimensionless time  $\tau = \omega_0 t / \sqrt{\varepsilon}$  corresponds to physical time  $\sqrt{\varepsilon}/\omega_0 \approx 2.8 \times 10^{-14}$  s, and the interval from  $\tau = 0$  to  $\tau = 6$ , shown on the figure, corresponds to the physical time interval  $\Delta t \approx 1.7 \times 10^{-13}$  s [2]. Thus, the applicability condition for the collisionless approximation, given by Eq. (24), is valid for these results. The simulations reveal that the colliding electromagnetic pulses temporarily merge, within time interval  $2.75 < \tau < 4.25$ , which is accompanied by fluctuations of the field energy density in a limited region of space. At the post-collision stage, the pulses separate and continue the propagation in a way similar to that before the collision. Lastly, it is worth adding that with the increase in the velocity, the collision between pulses becomes more elastic. The basic reason for this is that the collision time decreases.

Figure 3 shows the distribution of the energy density  $I(\xi, 0, \zeta, \tau)$  of the electric field in the array in the course of the propagation and interaction of the pulses in the plane of  $(\xi, \zeta)$  (at  $v = 0$ ): before the collision [Figs. 3(a) and 3(b)], and after the collision [Figs. 3(c) and 3(d)]. Note that the distribution of  $I(0, v, \tau)$  in the plane of



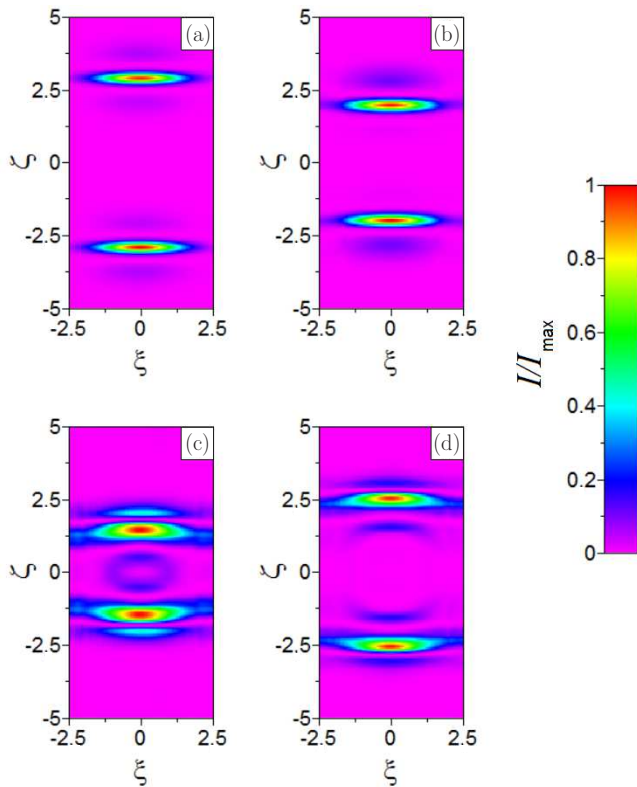


FIG. 3. The distribution of the energy density  $I(\xi, 0, \zeta, \tau)$  of the electric field in the plane of  $(\xi, \zeta)$  prior to and past the collision, at different times  $\tau$ : (a)  $\tau = 0.1$ , (b)  $\tau = 1.0$ , (c)  $\tau = 5.0$ , (d)  $\tau = 6.0$ . Values of  $I$  are color coded in the same way as in Fig. 2.

$(v, \zeta)$  is very similar to what is observed in the plane of  $(\xi, \zeta)$ . The energy density of the field is represented by ratio  $I/I_{\max}^{(\xi, \zeta)}$ , different values of which correspond to a variation of colors (flooded contours) from violet to red,  $I_{\max}^{(\xi, \zeta)}$  being the maximum value of the intensity at given time in the plane of  $(\xi, \zeta)$ . This figure shows stable propagation of the pulses in the array, without any conspicuous spreading.

Figure 4 shows, for clarity, the distribution of the energy density,  $I(0, 0, \zeta, \tau)$ , and the electric-field amplitude,  $E_{\parallel}(0, 0, \zeta, \tau)/E_0$ , of the pulses along the  $\zeta$  axis at some time  $\tau$ . Figures 2–4 clearly corroborate that both pulses propagate quite stably both before and after the collision. By the stability, we mean that the pulses pass, with a virtually undistorted shape, the distance considerably greater than their characteristic sizes along the propagation direction ( $\zeta$ ).

The simulations demonstrate that, in the course of the propagation of the pulses, their longitudinal and transverse widths may change, following decrease of the peak energy density. The reduction in the peak density may be explained by their dispersive spreading in the propagation direction ( $\zeta$ ), as well as by diffractive broadening in the orthogonal directions. Also, a part of the pulses'

energy goes into formation of “ripples” or “tails”, i.e., emission of small-amplitude waves. Nevertheless, in the entire parameter region considered in this work, these effects remain small and do not cause destruction of the pulses. Note also that, in this paper we consider the conservative model, in which the total energy remains constant, hence, attenuation of the pulses is not accounted for by dissipative losses.

Considering various factors that cause the change in the shape of the colliding pulses, we concluded that the pulses propagating toward each other induce dynamical spatiotemporal perturbations in the electron density and scalar potential,  $\eta$  and  $\Phi$  (similar effects in the spatial domain have been previously considered in Refs. [30, 38]). Thus, each pulse, coming into the spatial region already visited by the other one, experiences an impact from the perturbations left by the second pulse. In other words, the evolution of the electromagnetic field of the pulse is *indirectly* affected by the presence of the counterpropagating one, which leads to the *indirect* interaction between the pulses through the perturbations induced by them in the electronic subsystem of the CNT array.

### C. Redistribution of the electron density

As mentioned above, the propagation and interaction of the pulses result in significant redistribution of the conduction-electrons concentration. Figure 5 shows the distribution of the electron density before the collision. The electron density in the planes of  $(\xi, \zeta)$  and  $(v, \zeta)$  is represented by ratios  $(\eta - \eta_{\min}^{(\xi, \zeta)}) / (\eta_{\max}^{(\xi, \zeta)} - \eta_{\min}^{(\xi, \zeta)})$  and  $(\eta - \eta_{\min}^{(v, \zeta)}) / (\eta_{\max}^{(v, \zeta)} - \eta_{\min}^{(v, \zeta)})$ , respectively. Different values of the ratios correspond to a variation of colors from violet to red, similar to Fig. 2.

For comparison, Fig. 6 shows the distribution of the electron density in the course of the propagation of a single pulse, at the same moments of time. This figure clearly shows that the propagating pulse leaves behind a wake consisting of high- and low-density spots. Therefore, during the collision and thereafter, each pulse not only perturbs the medium, as seen in Fig. 6, but, as said above, it is forced to propagate in a medium which has already been perturbed by the counterpropagating pulse, which leads to the aforementioned indirect interaction between the pulses. The electron-concentration distribution after the collision [see Figs. 5(c) and (g) and 5(d) and (h)] is symmetric with respect to a plane drawn through the origin perpendicularly to the  $\zeta$  axis.

Note that the pulse velocities are high (somewhat smaller than the speed of light in the surrounding dielectric), therefore, they are actually exposed to the environment perturbed by the counterpropagating pulse for a very short of time, the corresponding perturbation in the electron density of the passing pulse being on the order of a few percent. As a result, the interaction affects the shape of the pulses, but does not lead to dramatic



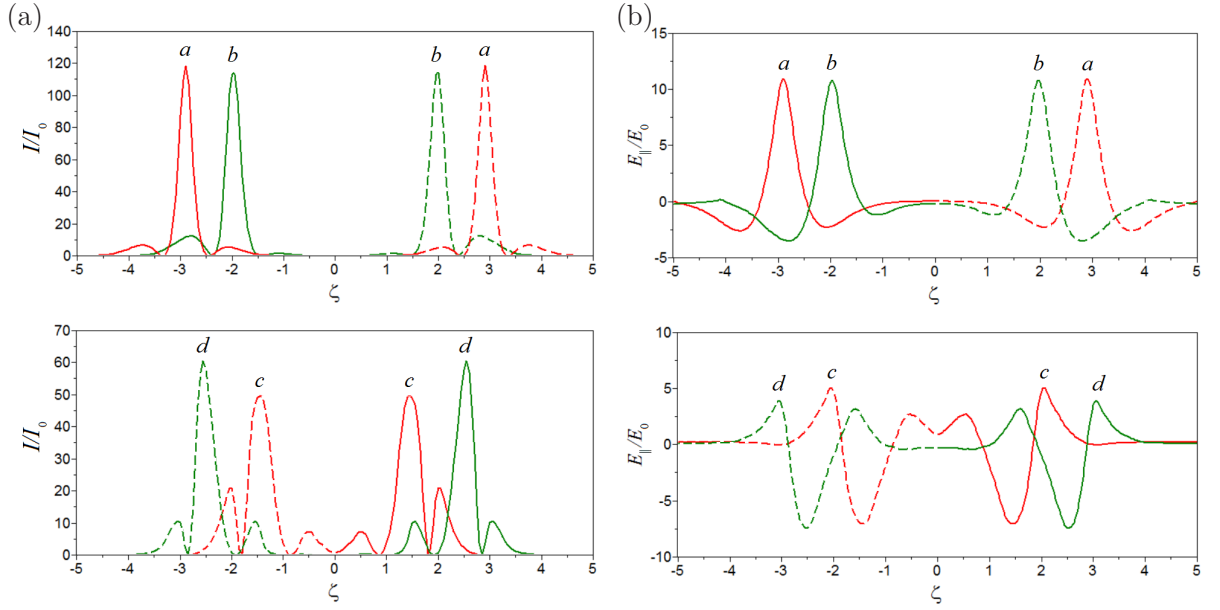


FIG. 4. (a): The intensity distribution of the pulses on the  $\zeta$  axis at different times  $\tau$ —before the collision, at  $\tau = 0.1$  (line  $a$ ),  $\tau = 1.0$  (line  $b$ ), and after the collision, at  $\tau = 5.0$  (line  $c$ ),  $\tau = 6.0$  (line  $d$ ). Dashed lines correspond to the counter-propagating pulse. (b): The same for the scaled electric field,  $E_{\parallel}/E_0$ .

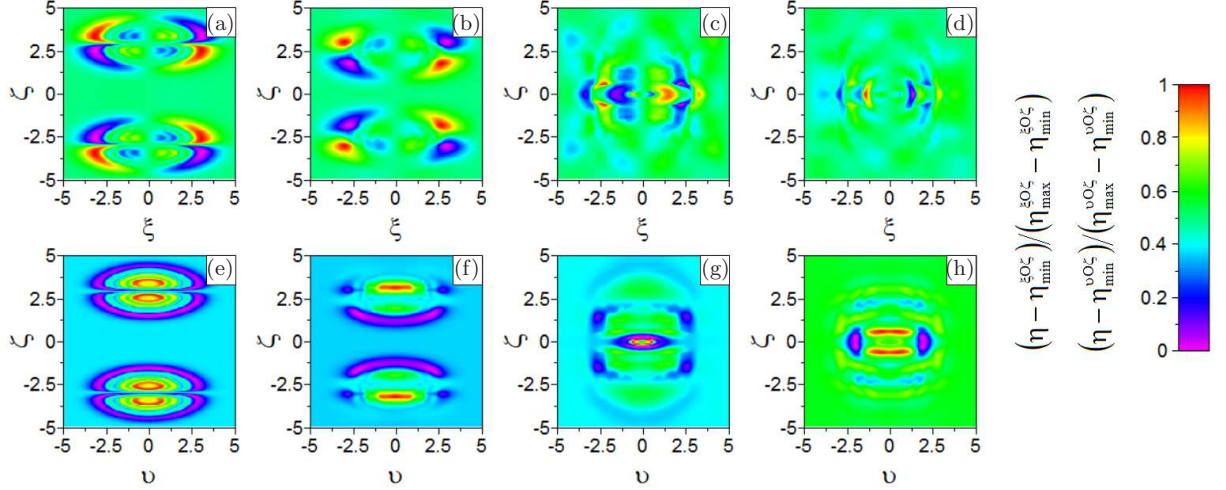


FIG. 5. Electron density distribution  $\eta(\xi, 0, \zeta, \tau)$  and  $\eta(0, v, \zeta, \tau)$  in planes  $(\xi, \zeta)$  and  $(v, \zeta)$ , respectively, before and after the collision of the electromagnetic pulses at different times: (a), (e)  $\tau = 0.1$ , (b), (f)  $\tau = 1.0$ , (c) and (g)  $\tau = 5.0$ , and (d), (h)  $\tau = 6.0$ . Different values of the concentration correspond to a variation of colors from violet (minimum) to red (maximum).

changes in their dynamics, and does not destabilize their propagation. Here, we have to emphasize that the primary goal of this study is to demonstrate that the pulses survive the collision, which may thus be considered as a quasi-elastic one. We do not address the stability over much longer propagation distances, which is a topic for a separate investigation.

Figure 7 shows a comparison of quantities  $I(0, 0, \zeta, \tau)$  and  $E(0, 0, \zeta, \tau)$  in two situations: (i) the single-pulse propagation, and (ii) the collision between the pulses. Naturally, the evolution of the shape of the solitary wave

interacting with the other pulse is somewhat different from the evolution in the case of a single pulse. The differences manifest themselves in the shape of both the solitary-waves' bodies and their tails trailing the bodies.

#### D. Evolution of the Poynting vector

Finally, we present the results produced by the simulations for the energy transfer associated with the propagation and interaction of the electromagnetic pulses in the

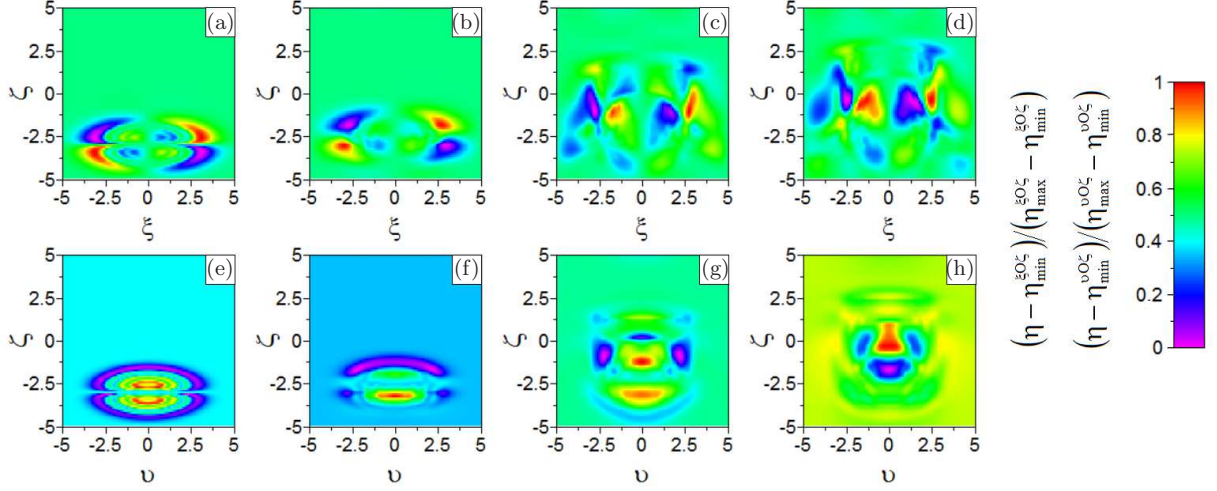


FIG. 6. Electron density distributions  $\eta(\xi, 0, \zeta, \tau)$  and  $\eta(0, v, \zeta, \tau)$  in the planes  $(\xi, \zeta)$  and  $(v, \zeta)$ , respectively, corresponding to a single propagating pulse, at different times: (a), (e)  $\tau = 0.1$ , (b), (f)  $\tau = 1.0$ , (c), (g)  $\tau = 5.0$ , and (d), (h)  $\tau = 6.0$ . Different values of the density correspond to a variation of colors from violet (minimum) to red (maximum).

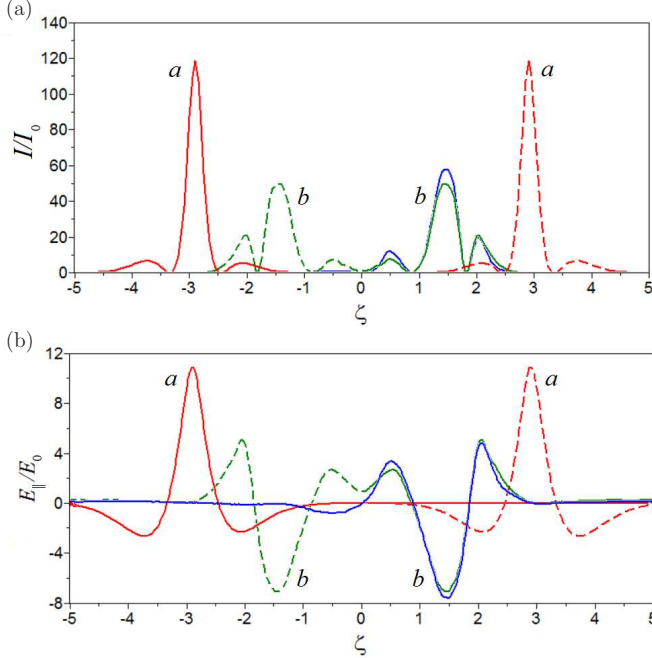


FIG. 7. (a): Intensity distribution  $I/I_0$  for different times. The solid red (resp. green) line  $a$  (resp.  $b$ ) shows the profile of the pulse before (resp. after) the collision at  $\tau = 0.1$  (resp. at  $\tau = 5.0$ ). The dashed lines represent the counterpropagating pulse at the same instant: red, before collision at  $\tau = 0.1$ , and green, after collision at  $\tau = 5.0$ . For the sake of comparison, the profile of the single pulse is shown by the blue line at  $\tau = 5.0$ . (b): The same for ratio  $E_{\parallel}/E_0$ .

system. As shown by the simulations, the strong inequality holds between components of the Poynting vector:  $|S_z| \gg |S_y| \gg |S_x|$ . Thus, the energy transfer is chiefly directed along the  $\zeta$  axis. This result reflects the fact

that the processes of the formation of “tails” extending in the transverse direction (along the  $\xi$  and  $v$  axes), as well as the transverse pulse broadening, are much weaker than the longitudinal energy transfer.

Figure 8 shows the distribution of the normalized  $z$ -component of the Poynting vector,  $S_z/S_0$  (see Appendix C for details) at different time instants  $\tau$ , prior to the collision between the pulses and afterwards. The figure is an alternative way of presenting the evolution of the shape of the electromagnetic pulses. For clarity,  $S_z/S_0$  is represented by lines of different colors (in the same way as in Figs. 4 and 7). Specifically, red indicates the profile of solitary waves before they hit each other, and green refers to the post-collision stage. Areas on the axis corresponding to the transfer of energy in the positive and negative directions of the  $\zeta$  axis are indicated by solid and dashed lines, respectively. The figure corroborates that the pulses retain their individuality after the collision, passing distances much greater than their own sizes.

Figure 8 allows us to evaluate the pulse’s energy flux along the propagation direction. For the given values of parameters, we find [see an explanation for Eq. (C5) in Appendix B]  $S_0 \approx 6.5 \times 10^9$  W/cm<sup>2</sup>, which corresponds to the unit on the vertical axis of Fig. 8. Thus, the maxima of  $|S_z|$  on the  $\zeta$  axis for each pulse before and after the collision yields  $7.1 \times 10^{11}$  W/cm<sup>2</sup> and  $3.2 \times 10^{11}$  W/cm<sup>2</sup>, respectively.

Some peculiarities of the propagation and interaction of the light bullets reported in this paper can possibly be used for the design of new elements of nanoscale optoelectronic devices and laser control systems, as well as for all-optical data processing. In particular, the effect of the redistribution of the electron density by an electromagnetic solitary wave suggests possibilities for the creation of CNT-based light-by-light control devices, uti-

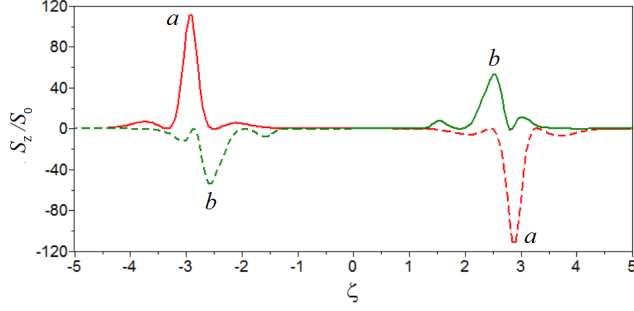


FIG. 8. The normalized Poynting-vector component,  $S_z/S_0$ , associated with the pulses' fields at different times  $\tau$ . The solid red (resp. green) line  $a$  (resp.  $b$ ) shows the profile of the pulse before (resp. after) the collision at  $\tau = 0.1$  (resp. at  $\tau = 6.0$ ). The dashed lines represent the counterpropagating pulse at the same instant: red, before collision at  $\tau = 0.1$ , and green, after collision at  $\tau = 5.0$ . Solid and dashed lines correspond, respectively, to the energy transfer in the positive and negative directions along the  $\zeta$  axis.

lizing the respective indirect interaction between the control and signal pulses. These perspectives for the use of CNT arrays are suggested by results of Refs. [50, 51] and [52]–[56], which predict strong transformation of radiation as a result of its reflection from solitons in a nonlinear medium, with dynamical nonuniformity of the refractive index moving along with the soliton. This effect may be probably used for the design of metamaterials with rapidly changing dynamical properties.

#### IV. CONCLUSIONS

Key results of this work may be summarized as follows:

- (i) The complete set of equations describing the evolution of the field and charge density were derived for the propagation and interaction of light bullets in the array of CNTs (semiconducting carbon nanotubes). Our modeling framework takes into account the perturbation of the electron density by the nonuniformity of the field along the CNT axis.
- (ii) The mechanism of the indirect interaction of extremely short electromagnetic pulses via the overlapping perturbations of the electron subsystem in the CNT array was thoroughly studied by using the visualization of two complementary quantities: the distribution of the energy density of the electric field, as a characteristic of the field localization, and components of the Poynting vector, as a characteristic of the propagation direction and energy flux.
- (iii) The numerical model used in this work allows the investigation of different scenarios of the interaction of bipolar electromagnetic pulses in the CNT

arrays. It has been established that the pulses separate after the collision, restoring their shape and steadily moving over distances much greater than their characteristic sizes.

- (iv) The electromagnetic pulses induce a dynamic perturbation of the electron density in the medium, which, in turn, affects the evolution of the electromagnetic waves in the environment. This mechanism may possibly have implications for the design of novel optoelectronic devices.

Finally, it is worth highlighting that our analysis is limited to the particular case of a strictly conservative system. Our estimates show that including effects associated with more realistic composites can lead to slight quantitative changes in the results, although the qualitative description remains unchanged.

#### AUTHORS' CONTRIBUTION STATEMENT

All the authors contributed equally to this work.

#### ACKNOWLEDGMENTS

A. V. Zhukov and R. Bouffanais are financially supported by the SUTD-MIT International Design Centre (IDC). N. N. Rosanov acknowledges the support from the Russian Foundation for Basic Research, Grant No. 16-02-00762, and from the Foundation for the Support of Leading Universities of the Russian Federation (Grant No. 074-U01). M. B. Belonenko acknowledges support from the Russian Foundation for Fundamental Research. E. G. Fedorov is grateful to Professor T. Shemesh for his generous support. B. A. Malomed appreciates hospitality of the School of Electrical and Electronic Engineering at the Nanyang Technological University (Singapore).

### Appendix A: Derivation of the dispersion relation for linear waves in the system

The full system of evolution equations is

$$\frac{\partial^2 \Psi}{\partial \tau^2} - \left( \frac{\partial^2 \Psi}{\partial \xi^2} + \frac{\partial^2 \Psi}{\partial v^2} + \frac{\partial^2 \Psi}{\partial \zeta^2} \right) + \eta \sum_{r=1}^{\infty} G_r \sin \left[ r \left( \Psi + \int_0^{\tau} \frac{\partial \Phi}{\partial \xi} d\tau' \right) \right] = 0, \quad (\text{A1})$$

$$\frac{\partial^2 \Phi}{\partial \tau^2} - \left( \frac{\partial^2 \Phi}{\partial \xi^2} + \frac{\partial^2 \Phi}{\partial v^2} + \frac{\partial^2 \Phi}{\partial \zeta^2} \right) = \beta(\eta - 1), \quad (\text{A2})$$

$$\frac{\partial \eta}{\partial \tau} = \alpha \sum_{r=1}^{\infty} G_r \frac{\partial}{\partial \xi} \left\{ \eta \sin \left[ r \left( \Psi + \int_0^{\tau} \frac{\partial \Phi}{\partial \xi} d\tau' \right) \right] \right\}. \quad (\text{A3})$$

The linearization of Eqs. (A1) and (A3) is performed on top of the trivial solution,  $\Psi = \Phi = 0$ ,  $\eta = 1$ , and (for the time being) only the first harmonic is kept in the Fourier series in Eqs. (A1) and (A3) [Eq. (A2) is linear by itself]:

$$\frac{\partial^2 \Psi}{\partial \tau^2} - \left( \frac{\partial^2 \Psi}{\partial \xi^2} + \frac{\partial^2 \Psi}{\partial v^2} + \frac{\partial^2 \Psi}{\partial \zeta^2} \right) + G_1 \left( \Psi + \int_0^{\tau} \frac{\partial \Phi}{\partial \xi} d\tau' \right) = 0, \quad (\text{A4})$$

$$\frac{\partial \eta}{\partial \tau} - \alpha G_1 \frac{\partial}{\partial \xi} \left( \Psi + \int_0^{\tau} \frac{\partial \Phi}{\partial \xi} d\tau' \right) = 0. \quad (\text{A5})$$

Further, we define

$$\theta \equiv \eta - 1, \quad (\text{A6})$$

$$\varphi \equiv \int_0^{\tau} \frac{\partial \Phi}{\partial \xi} d\tau', \quad (\text{A7})$$

hence

$$\frac{\partial \Phi}{\partial \xi} \equiv \frac{\partial \varphi}{\partial \tau}, \quad (\text{A8})$$

and replace Eq. (A2) by the equation differentiated with respect to  $\xi$ :

$$\begin{aligned} & \beta \frac{\partial \theta}{\partial \xi} - \frac{\partial^2}{\partial \tau^2} \left( \frac{\partial \Phi}{\partial \xi} \right) \\ & + \frac{\partial^2}{\partial \xi^2} \left( \frac{\partial \Phi}{\partial \xi} \right) + \frac{\partial^2}{\partial v^2} \left( \frac{\partial \Phi}{\partial \xi} \right) + \frac{\partial^2}{\partial \zeta^2} \left( \frac{\partial \Phi}{\partial \xi} \right) = 0. \end{aligned} \quad (\text{A9})$$

Then,  $\partial \Phi / \partial \xi$  in Eq. (A9) is replaced by  $\partial \varphi / \partial \tau$ , according to Eqs. (A8), and definition (A7) is used in Eqs. (A4) and (A5). Thus, the linearized equations are cast in their final form:

$$\frac{\partial \theta}{\partial \tau} - \alpha G_1 \frac{\partial \varphi}{\partial \xi} - \alpha G_1 \frac{\partial \Psi}{\partial \xi} = 0. \quad (\text{A10})$$

$$\beta \frac{\partial \theta}{\partial \xi} - \frac{\partial^3 \varphi}{\partial \tau^3} + \frac{\partial^3 \varphi}{\partial \tau \partial \xi^2} + \frac{\partial^3 \varphi}{\partial \tau \partial v^2} + \frac{\partial^3 \varphi}{\partial \tau \partial \zeta^2} = 0, \quad (\text{A11})$$

$$G_1\varphi + G_1\Psi + \frac{\partial^2\Psi}{\partial\tau^2} - \left( \frac{\partial^2\Psi}{\partial\xi^2} + \frac{\partial^2\Psi}{\partial v^2} + \frac{\partial^2\Psi}{\partial\zeta^2} \right) = 0. \quad (\text{A12})$$

Solutions to linearized equations (A10) and (A11) are looked for in the usual form,

$$(\theta, \varphi, \Psi) \sim \exp(-iF\tau + iK\xi + iPv + iQ\zeta), \quad (\text{A13})$$

where  $K, P, Q$  are arbitrary wave numbers, and  $F$  is the frequency to be found. The substitution of ansatz (A13) in Eqs. (A10) and (A11) leads to the dispersion equation, written in the determinant form:

$$\begin{vmatrix} -iF & -i\alpha G_1 K & -i\alpha G_1 K \\ i\beta K & iF^3 + iF(K^2 + P^2 + Q^2) & 0 \\ 0 & G_1 & G_1 - F^2 + (K^2 + P^2 + Q^2) \end{vmatrix} = 0. \quad (\text{A14})$$

In an explicit form, Eq. (A14) is a cubic equation for  $F^2$ :

$$\begin{aligned} & (F^2)^3 - G_1 (F^2)^2 \\ & - F^2 [(K^4 + P^4 + Q^4) + 2(K^2 P^2 + K^2 Q^2 + P^2 Q^2) + G_1 (K^2 + P^2 + Q^2) + \alpha\beta G_1 K^2] \\ & + \alpha\beta G_1 (K^4 + K^2 P^2 + K^2 Q^2) = 0. \end{aligned} \quad (\text{A15})$$

In the limit of  $K^2, P^2, Q^2 \rightarrow \infty$ , a relevant dispersion branch is given by an asymptotic solution to Eq. (A15)

$$F^2 \approx \sqrt{(K^4 + P^4 + Q^4) + 2(K^2 P^2 + K^2 Q^2 + P^2 Q^2)}. \quad (\text{A16})$$

The main objective is to obtain a band gap from a numerical analysis of Eq. (A15), that would be a habitat for solitons. It seems that the band gap *does not exist*, because, in the limit of  $K^2, P^2, Q^2 \rightarrow 0$ , the asymptotic form of Eq. (A15) is

$$(F^2)^2 + F^2 [(K^2 + P^2 + Q^2) + \alpha\beta K^2] - \alpha\beta K^2 (K^2 + P^2 + Q^2) = 0, \quad (\text{A17})$$

Obviously, Eq. (A17) shows that, in this limit, the spectrum does not contain a band gap, but rather a Dirac cone (which is not surprising for a medium related to graphene). Sometimes, solitons may actually exist or “almost exist” in the absence of a true band gap [57]. In fact, it is a separate problem to check if solitons exist in the present model in the strict mathematical sense.

## Appendix B: Computation of the conduction current

Here we aim to derive an expression for the conduction-current density  $j$  along the CNT axis, applying an approach similar to the one used in Refs. [44, 45] for semiconductor superlattices. Assuming the variation length of the electromagnetic field to be much larger than the electron de Broglie wavelength and length  $d_x$  in the electron dispersion law (1), we write the current density, associated with the motion of the conduction electrons, as

$$j = 2e \sum_{s=1}^m \int_{-\pi\hbar/d}^{+\pi\hbar/d} v_x(p_x + p_0, s) f(p_x, s) dp_x. \quad (\text{B1})$$

Here  $v_x$  is the electron's velocity, and  $f(p_x, s)$  is the associated distribution function. The integration with respect to quasimomentum  $p_x$  is carried out over the interval between  $-\pi\hbar/d$  and  $+\pi\hbar/d$  (note that  $p_x/\hbar$  thus varies within the first Brillouin zone), and  $p_0$  is determined by the equation of motion,

$$\frac{dp_0}{dt} = - \left( \frac{e}{c} \frac{\partial A}{\partial t} + e \frac{\partial \phi}{\partial x} \right). \quad (\text{B2})$$

It follows from Eq. (B2) that

$$p_0 = - \left( \frac{e}{c} A + e \int_0^t \frac{\partial \phi}{\partial x} dt' \right). \quad (\text{B3})$$

Next, to continue the derivation of the current density by means of Eq. (B1), we need an expression for the velocity of the electrons,  $v_x(p_x + p_0, s)$ . To this end, we use the known definition,  $v_x(p_x, s) = \partial\epsilon(p_x, s)/\partial p_x$ . The expression for  $v_x(p_x, s)$  being available, we make a substitution,  $p_x \rightarrow p_x + p_0$ , to obtain  $v_x(p_x + p_0, s)$ .

Next we expand the electron spectrum  $\epsilon(p_x, s)$  in the Fourier series:

$$\epsilon(p_x, s) = \frac{\delta_{0,s}}{2} + \sum_{r=1}^{\infty} \delta_{r,s} \cos\left(r \frac{d_x}{\hbar} p_x\right), \quad (\text{B4})$$

$$\delta_{r,s} = \frac{d_x}{\pi\hbar} \int_{-\pi\hbar/d}^{\pi\hbar/d} \epsilon(p_x, s) \cos\left(r \frac{d_x}{\hbar} p_x\right) dp_x. \quad (\text{B5})$$

Using expression (B4) for the electron energy spectrum, we rewrite the electron velocity  $v_x(p_x, s)$  as

$$v_x(p_x, s) = \frac{\partial\epsilon(p_x, s)}{\partial p_x} = -\frac{d_x}{\hbar} \sum_{r=1}^{\infty} r \delta_{r,s} \sin\left(r \frac{d_x}{\hbar} p_x\right). \quad (\text{B6})$$

Making the substitution  $p_x \rightarrow p_x + p_0$  in Eq. (B6), we can rewrite current density (B1):

$$j = -2e \frac{d_x}{\hbar} \sum_{s=1}^m \int_{-\pi\hbar/d}^{\pi\hbar/d} \sum_{r=1}^{\infty} r \delta_{r,s} \sin\left\{r \frac{d_x}{\hbar} (p_x + p_0)\right\} f(p_x, s) dp_x. \quad (\text{B7})$$

Further, we make use of the Fermi-Dirac distribution

$$f(p_x, s) = \frac{N}{1 + \exp\left(\frac{\epsilon(p_x, s)}{k_B T}\right)}, \quad (\text{B8})$$

where  $N$  is the constant determined from the normalization condition,

$$2 \sum_{s=1}^m \int_{-\pi\hbar/d}^{\pi\hbar/d} f(p_x, s) dp_x = n, \quad (\text{B9})$$

where pre-factor 2 accounts for the two possible electron spin projections. We stress that the conduction-electron density  $n$  in Eq. (B9) is, generally, a function of the spatial coordinates and time,  $n = n(x, z, t)$ .

Now we transform the current density given by Eq. (B7), taking into regard the distribution function (B8) and normalization condition (B9):

$$j = -\gamma_0 e \frac{d_x}{\hbar} n \sum_{r=1}^{\infty} G_r \sin\left\{r \frac{d_x}{\hbar} \left(\frac{e}{c} A + e \int_0^t \frac{\partial\phi}{\partial x} dt'\right)\right\}, \quad (\text{B10})$$

$$G_r = -r \frac{\sum_{s=1}^m (\delta_{r,s}/\gamma_0) \int_{-\pi\hbar/d}^{+\pi\hbar/d} \cos\left(r \frac{d_x}{\hbar} p_x\right) \left[1 + \exp\left(\frac{\epsilon(p_x, s)}{k_B T}\right)\right]^{-1} dp_x}{\sum_{s=1}^m \int_{-\pi\hbar/d}^{+\pi\hbar/d} \left\{1 + \exp\left(\frac{\epsilon(p_x, s)}{k_B T}\right)\right\}^{-1} dp_x}. \quad (\text{B11})$$

Using an expression for the electron spectrum following from Eq. (B4), we finally obtain

$$G_r = -r \frac{\sum_{s=1}^m (\delta_{r,s}/\gamma_0) \int_{-\pi\hbar/d}^{+\pi\hbar/d} \cos\left(r \frac{d_x}{\hbar} p_x\right) \left[1 + \exp\left(\frac{\delta_{0,s}}{2k_B T} + \sum_{q=1}^{\infty} \frac{\delta_{q,s}}{k_B T} \cos\left(q \frac{d_x}{\hbar} p_x\right)\right)\right]^{-1} dp_x}{\sum_{s=1}^m \int_{-\pi\hbar/d}^{+\pi\hbar/d} \left[1 + \exp\left(\frac{\delta_{0,s}}{2k_B T} + \sum_{q=1}^{\infty} \frac{\delta_{q,s}}{k_B T} \cos\left(q \frac{d_x}{\hbar} p_x\right)\right)\right]^{-1} dp_x}. \quad (\text{B12})$$

Finally, with substitution  $p_x d_x/\hbar \rightarrow \kappa$  and notation  $\theta_{r,s} = \delta_{r,s}(k_B T)^{-1}$ , we obtain expression (4) used in the main text.

### Appendix C: The Poynting vector

The redistribution of the energy density of energy in the system in the course of motion and transformation of the solitary waves can be described by analyzing the evolution of the Poynting vector, i.e., the vector of the energy-flux density of the electromagnetic field [40, 41]:

$$\mathbf{S} = (c/4\pi) \mathbf{E} \times \mathbf{H}. \quad (\text{C1})$$

We assume that the medium under consideration is nonmagnetic, with relative permeability 1. In this case, the magnetic component of the field, being expressed in terms of the vector potential as  $\mathbf{H} = \nabla \times \mathbf{A}$ , can be written as

$$\mathbf{H} = H_0 \left( 0, \frac{\partial \Psi}{\partial \zeta}, -\frac{\partial \Psi}{\partial v} \right), \quad (\text{C2})$$

where  $H_0 = -\hbar\omega_0(ed_x)^{-1}$ .

Thus, calculating the vector product of the electric (11) and magnetic (C2) fields, we find the Poynting vector,  $\mathbf{S} = \{S_x, S_y, S_z\}$ , with the following components:

$$S_x = S_0 \left( \frac{\partial \Phi}{\partial v} \frac{\partial \Psi}{\partial v} + \frac{\partial \Phi}{\partial \zeta} \frac{\partial \Psi}{\partial \zeta} \right), \quad (\text{C3})$$

$$S_y = -S_0 \frac{\partial \Psi}{\partial v} \left( \frac{\partial \Psi}{\partial \tau} + \frac{\partial \Phi}{\partial \xi} \right), \quad (\text{C4})$$

$$S_z = -S_0 \frac{\partial \Psi}{\partial \zeta} \left( \frac{\partial \Psi}{\partial \tau} + \frac{\partial \Phi}{\partial \xi} \right), \quad (\text{C5})$$

where  $S_0 = (c/4\pi)(\hbar\omega_0)^2(ed_x)^{-2}\varepsilon^{-1/2}$ .

Computation of the absolute value of the Poynting vector allows us to find the density of the field's energy flux at each point and any instant of time. The direction of the power transfer is determined by signs of the components of  $\mathbf{S}$ :  $\text{sign}(S_x)$ ,  $\text{sign}(S_y)$ ,  $\text{sign}(S_z)$ . The energy transfer associated with the motion of the electromagnetic pulses and the formation of their tails along the  $\zeta$  axis is determined by the corresponding component  $S_z$ , given by Eq. (C5). The energy transfer along the  $\zeta$  and  $v$  axes, which can also contribute to a change in the shape of the pulse, is determined by components  $S_x$  [(C3)] and  $S_y$  [(C4)], respectively. The simulations show that the strong inequality between projections holds,  $|S_z| \gg |S_y| \gg |S_x|$ , hence, the energy transfer occurs chiefly along the  $\zeta$  axis. This result reflects the fact that the formation of the tails in the transverse directions (along  $\xi$  and  $v$ ), as well as transverse pulse broadening, are much weaker than the longitudinal energy transfer associated with the propagation of the pulses along the  $\zeta$  axis.

- 
- |  |   |
|--|---|
| <p>[1] R. H. Baughman, A. A. Zakhidov, and W. A. de Heer, <i>Science</i> <b>297</b>, 787 (2002).</p> <p>[2] S. Iijima, <i>Nature</i> <b>354</b>, 56 (1991).</p> <p>[3] S. Iijima and T. Ichihashi, <i>Nature</i> <b>363</b>, 603 (1993).</p> <p>[4] M. S. Dresselhaus, G. Dresselhaus, P. Eklund, <i>The science of fullerenes and carbon nanotubes</i> (Elsevier, 1996).</p> <p>[5] <i>Carbon nanotubes, preparation and properties</i>, T. W. Ebbesen, Ed. (CRC Press, 1996).</p> <p>[6] R. Saito, G. Dresselhaus, and M. S. Dresselhaus, <i>Physical properties of carbon nanotubes</i> (World Scientific, 1998).</p> <p>[7] P. J. F. Harris, <i>Carbon Nanotubes and Related Structures: New Materials for the Twenty-First Century</i> (Cambridge University Press, 1999).</p> <p>[8] S. A. Maksimenko and G. Ya. Slepian, <i>J. Comm. Techn. Elect.</i> <b>47</b>, 261 (2002).</p> | <p>[9] S. A. Maksimenko and G. Ya. Slepian, in <i>Handbook of Nanotechnology. Nanometer Structure: Theory, Modeling, and Simulation</i> (SPIE Press, Bellingham, 2004).</p> <p>[10] A. Akhmanov, V. A. Vysloukh, and A. S. Chirkin, <i>Optics of Femtosecond Laser Pulses</i> (AIP, New York, 1992).</p> <p>[11] F. G. Bass, A. A. Bulgakov, A. P. Teterov, <i>High-frequency properties of semiconductors with superlattices</i> (Nauka, Moscow, 1989).</p> <p>[12] M. A. Herman, <i>Semiconductor Superlattices</i> (Akademie-Verlag, 1986).</p> <p>[13] M. B. Belonenko, S. Yu. Glazov, and N. E. Meshcheryakova, <i>Bull. Rus. Acad. Sci: Physics</i> <b>73</b>, 1601 (2009).</p> <p>[14] M. B. Belonenko, N. G. Lebedev, and N. N. Yanyushkina, <i>J. Rus. Laser Res.</i> <b>31</b>, 410 (2010).</p> <p>[15] A. V. Zhukov, R. Bouffanais, M. B. Belonenko, and E. G. Fedorov, <i>Mod. Phys. Lett. B</i> <b>27</b>, 1350045 (2013).</p> |
|--|---|



- [16] M. B. Belonenko, E. G. Fedorov, *Rus. Phys. J.* **55**, 83 (2012).
- [17] M. B. Belonenko, E. V. Demushkina, and N. G. Lebedev, *J. Rus. Laser Res.* **27**, 457 (2006).
- [18] A. M. Zheltikov, *Phys.-Usp.* **50**, 705 (2007).
- [19] S. V. Sazonov, *Bull. Rus. Acad. Sci.: Physics* **75**, 157 (2011).
- [20] H. Leblond and D. Mihalache, *Phys. Rep.* **523**, 61 (2013).
- [21] G. Mourou, S. Mironov, E. Khazanov, and A. Sergeev, *Eur. Phys. J. Special Topics*, **223**, 1181 (2014).
- [22] M. Kolesik and J. V. Moloney, *Rep. Prog. Phys.* **77**, 016401 (2014).
- [23] D. J. Frantzeskakis, H. Leblond, and D. Mihalache, *Rom. J. Phys.* **59**, 767 (2014).
- [24] M. B. Belonenko, N. G. Lebedev, and A. S. Popov, *JETP Lett.* **91**, 461 (2010).
- [25] E. G. Fedorov, A. V. Zhukov, M. B. Belonenko, and T. F. George, *Eur. Phys. J. D* **66**, 219 (2012).
- [26] H. Leblond and D. Mihalache, *Phys. Rev. A* **86**, 043832 (2012).
- [27] B. A. Malomed, D. Mihalache, F. Wise, and L. Torner, *J. Opt. B.: Quantum Semiclass. Opt.* **7**, R53 (2005).
- [28] D. Mihalache, *Rom. J. Phys.* **57**, 352 (2012).
- [29] D. Mihalache, *Rom. J. Phys.* **59**, 295 (2014).
- [30] A. V. Zhukov, R. Bouffanais, E. G. Fedorov, and M. B. Belonenko, *J. Appl. Phys.* **114**, 143106 (2013).
- [31] M. B. Belonenko, N. G. Lebedev, and N. N. Yanyushkina, *Phys. Sol. State*, **52**, 1780 (2010).
- [32] M. B. Belonenko, A. S. Popov, N. G. Lebedev, A. V. Pak, and A. V. Zhukov, *Phys. Lett. A* **375**, 946 (2011).
- [33] E. G. Fedorov, N. N. Konobeeva, and M. B. Belonenko, *Rus. J. Phys. Chem. B*, **8**, 409 (2014).
- [34] M. B. Belonenko, A. S. Popov, and N. G. Lebedev, *Tech. Phys. Lett.* **37**, 119 (2011).
- [35] A. S. Popov, M. B. Belonenko, N. G. Lebedev, A. V. Zhukov, and M. Paliy, *Eur. Phys. J. D* **65**, 635 (2011).
- [36] A. S. Popov, M. B. Belonenko, N. G. Lebedev, A. V. Zhukov, and T. F. George, *Int. J. Theor. Phys. Group Theory Nonlinear Opt.* **15**, 5 (2011).
- [37] A. V. Zhukov, R. Bouffanais, E. G. Fedorov, and M. B. Belonenko, *J. App. Phys.* **115**, 203109 (2014).
- [38] A. V. Zhukov, R. Bouffanais, H. Leblond, D. Mihalache, E. G. Fedorov, and M. B. Belonenko, *Eur. Phys. J. D* **69**, 242 (2015).
- [39] M. B. Belonenko, S. Yu. Glazov, and N. E. Meshcheryakova, *Opt. Spectr.* **108**, 774 (2010).
- [40] L. D. Landau and E. M. Lifshitz, *The Classical Theory of Fields*, 4th Ed. (Butterworth-Heinemann, Oxford, 2000).
- [41] L. D. Landau, E. M. Lifshitz, and L. P. Pitaevskii, *Electrodynamics of Continuous Media*, 2nd Ed. (Elsevier, Oxford, 2004).
- [42] W. Baumjohann and R. A. Treumann, *Basic Space Plasma Physics* (Imperial College Press, London, 1997).
- [43] G. Dong, J. Zhu, W. Zhang, and B. A. Malomed, *Phys. Rev. Lett.* **110**, 250401 (2013); J. Qin, G. Dong, and B. A. Malomed, *ibid.* **115**, 023901 (2015).
- [44] E. M. Epshtein, *Fiz. Tverd. Tela* **19**, 3456 (1976).
- [45] E. M. Epshtein, *Fiz. Tech. Polupr.* **14**, 2422 (1980) [*Sov. Phys. Semiconductors* **14**, 1438 (1980)].
- [46] A. N. Pikhtin, *Optical and Quantum Electronics* (High School Publishers, Moscow, 2001).
- [47] *Femtosecond Laser Pulses: Principles and Experiments*, Claude Rullière, ed. (Springer-Verlag, Berlin, 1998).
- [48] Yu. S. Kivshar and B. A. Malomed, *Rev. Mod. Phys.* **61**, 763 (1989).
- [49] J. W. Thomas, *Numerical Partial Differential Equations – Finite Difference Methods* (Springer-Verlag, New York, 1995).
- [50] N. N. Rosanov, *JETP Lett.* **88**, 501 (2008).
- [51] N. N. Rosanov, *JETP Lett.* **90**, 428 (2009).
- [52] A. Efimov, A. V. Yulin, D. V. Skryabin, J. C. Knight, N. Joly, F. G. Omenetto, A. J. Taylor, and P. Russell, *Phys. Rev. Lett.* **95**, 213902 (2005).
- [53] A. Efimov, A. J. Taylor, A. V. Yulin, D. V. Skryabin, and J. C. Knight, *Opt. Lett.* **31**, 1624 (2006).
- [54] R. Driben, A. V. Yulin, A. Efimov, and B. A. Malomed, *Opt. Exp.* **21**, 19091 (2013).
- [55] I. Oreshnikov, R. Driben, and A. V. Yulin, *Opt. Lett.* **40**, 5554 (2015).
- [56] Z. Deng, X. Fu, J. Liu, C. Zhao, and S. Wen, *Opt. Exp.* **24**, 10302 (2016).
- [57] N. Flytzanis and B. A. Malomed, *Phys. Lett. A* **227**, 335-339 (1997).